Scintillation induced response in passively-quenched Si-based single photon counting avalanche diode arrays

Virginia Ch. Spanoudaki[1] **and Craig S. Levin**[1,2,*]

[1]*Molecular Imaging Program at Stanford (MIPS) and Radiology Department, Stanford University School of Medicine, Stanford, California, USA*
[2]*Departments of Physics and Electrical Engineering, Stanford University, Stanford, California, USA*
[*]*cslevin@stanford.edu*

Abstract: An optical electrical model which studies the response of Si-based single photon counting arrays, specifically silicon photomultipliers (SiPMs), to scintillation light has been developed and validated with analytically derived and experimental data. The scintillator-photodetector response in terms of relative pulse height, 10%-90% rise/decay times to light stimuli of different rise times (ranging from 0.1 to 5 ns) and decay times (ranging from 1 to 50 ns), as well as for different decay times of the photodetector are compared in theory and simulation. A measured detector response is used as a reference to further validate the model and the results show a mean deviation of simulated over measured values of 1%.

OCIS codes: (040.1345) Avalanche photodiodes (APDs); (040.5160) Photodetectors; (040.1240) Arrays; (290.5930) Scintillation; (130.5990) Semiconductors.

References and links

1. G. F. Knoll, *Radiation detection and measurement*, (Wiley, 2001).
2. H. Peng and C. S. Levin, "Design study of a high-resolution breast-dedicated PET system built from cadmium zinc telluride detectors," Phys. Med. Biol. **54,** 2761–2788 (2010).
3. O. Thomas, Z. L. Yuan, J. F. Dynes, A. W. Sharpe, and A. J. Shields, "Efficient photon number detection with silicon avalanche photodiodes," Appl. Phys. Lett. **97,** 031102 (2010).
4. P. Eraerds, M. Legre, A. Rochas, H. Zbinden, and N. Gisin "SiPM for fast Photon-Counting and Multiphoton Detection," Opt. Express **15,** 14539–14549 (2007).
5. M. Akiba, K. Tsujino, K. Sato, and M. Sasaki " Multipixel silicon avalanche photodiode with ultralow dark count rate at liquid nitrogen temperature," Opt. Express **17,** 16885–16897 (2009).
6. N. Namekata, S. Adachi, and S. Inoue "1.5 GHz single-photon detection at telecommunication wavelengths using sinusoidally gated InGaAs/InP avalanche photodiode," Opt. Express **17,** 6275–6282 (2009).
7. Z. L. Yuan, A. W. Sharpe, L. F. Dynes, A. R. Dixon, and A. J. Shields, "Multi-gigahertz operation of photon counting InGaAs avalanche photodiodes," Appl. Phys. Lett. **96,** 071101 (2010).
8. D.-U. Li, J. Arlt, J. Richardson, R. Walker, A. Buts, D. Stoppa, E. Charbon, and R. Henderson, "Real-time fluorescence lifetime imaging system with a 32×32 0.13μm CMOS low dark-count single-photon avalanche diode array," Opt. Express **18,** 10257–10269 (2010).
9. V. Ch. Spanoudaki and C. S. Levin "Investigating the temporal resolution limits of scintillation detection from pixelated elements: comparison between experiment and simulation," Phys. Med. Biol. in press (2011).
10. F. Corsi, A. Dragone, C. Marzocca, A. Del Guerra, P. Delizia, N. Dinu, C. Piemonte, M. Boscardin, and G. F. Dalla Betta, "Modeling a silicon photomultiplier (SiPM) as a signal source for optimum front-end design," Nucl. Instrum. Methods Phys. Res. A **572,** 416–418 (2007).
11. F. Zappa, A. Tosi, A. Dalls Mora, and S. Tisa "SPICE modeling of single photon avalanche diodes," Sens. Actuators A Phys. **153,** 197–204 (2009).

#139633 - $15.00 USD Received 14 Dec 2010; accepted 7 Jan 2011; published 13 Jan 2011

12. S. Seifert, H. T. van Dam, J. Huizenga, R. Vinke, P. Dendooven, H. Löhner, and D. Schaart "Simulation of Silicon Photomultipliers," IEEE Trans. Nucl. Sci. **56,** 3726–3733 (2009).
13. P. J. Hambleton, S. A. Plimmer, J. P. R. David, and G. J. Rees "Simulated current response in avalanche photodiodes," J. Appl. Opt. **91,** 2107–2111 (2002).
14. V. Ch. Spanoudaki and C. S. Levin "Photo-Detectors for Time of Flight Positron Emission Tomography (ToF-PET)," Sensors **10,** 10484–10505 (2010).
15. S. Cova, M. Ghioni, A. Lacaita, and F. Zappa "Avalanche photodiodes and quenching circuits for single-photon detection," Appl. Opt. **35,** 1956–1976 (1996).
16. S. Tisa, F. Guerrieri, and F. Zappa "Variable-Load Quenching Circuit for single-photon avalanche diodes," Opt. Express **16,** 2232–2244 (2008).
17. R. G. W. Brown, K. D. Ridley, and J. G. Rarity "Characterization of silicon avalanche photodiodes for photon correlation measurements. 1: Passive quenching," Appl. Opt. **25,** 4122–4126 (1986).
18. R. G. W. Brown, R. Jones, K. D. Ridley, and J. G. Rarity "Characterization of silicon avalanche photodiodes for photon correlation measurements. 2: Active quenching," Appl. Opt. **26,** 2383–2389 (1987).
19. G. Bonanno, P. Finocchiaro, A. Pappalardo, S. Billotta, L. Cosentino, M. Belluso, S. Di Mauro, and G. Occhipinti "Precision measurements of Photon Detection Efficiency for SiPM detectors," Nucl. Instrum. Methods Phys. Res. A **610,** 93–97 (2009).
20. Linear Technologies, `http://www.linear.com/designtools/software/ltspice.jsp`.
21. F. Cayouette, D. Laurendeau, and C. Moisan "DETECT2000: An Improved Monte-Carlo Simulator for the Computer Aided Design of Photon Sensing Devices," Proc. SPIE **4833,** 69 (2003).
22. J. S. Ng, C. H. Tan, J. P. R. David, and G. J. Rees "A general method for estimating the duration of avalanche multiplication," Semicond. Sci. Technol. **17,** 1067–1071 (2002).
23. S. M. Sze *Physics of semiconductor devices* (Wiley, New York,1981).
24. T. Szczesniak, M. Moszynski, A. Syntfeld-Kazuch, L. Swiderski, M. A. Spurrier Koschan, and C. L. Melcher "Timing Resolution and Decay Time of LSO Crystals Co-Doped With Calcium," IEEE Trans. Nucl. Sci. **57,** 1329–1334 (2010).
25. A. Nassalski, M. Moszynski, A. Syntfeld-Kazuch, T. Szczesniak, L. Swiderski, D. Wolski, and J. Baszak "Multi Pixel Photon Counters (MPPC) as an Alternative to APD in PET Applications," IEEE Trans. Nucl. Sci. **57,** 1008–1014 (2010).
26. A. Syntfeld-Kazuch, M. Moszynski, L. Swiderski, T. Szczesniak, A. Nassalski, C. L. Melcher, M. A. Spurrier, B. Goliszek, P. Kaminski, and M. Nowaczyk "Energy Resolution of Calcium Co-Doped LSO:Ce Scintillators," IEEE Trans. Nucl. Sci. **56,** 2972–2978 (2009).
27. I. Rech, A. Ingargiola, R. Spinelli, I. Labanca, S. Marangoni, M. Ghioni, and S. Cova "Optical crosstalk in single photon avalanche diode arrays: a new complete model," Opt. Express **16,** 8381–8394 (2008).
28. Y. Kang, H. X. Lu, and Y.-H. Lo "Dark count probability and quantum efficiency of avalanche photodiodes for single-photon detection," Appl. Phys. Lett. **83,** 2955–2957 (2003).

1. Introduction

In most modern imaging techniques the outcome is the result of an acquisition chain which eventually is reduced to the manipulation of electrical signals. In radionuclide imaging the electrical signals to be processed originate, in most cases, from a two-step conversion of the radiation quantum to visible light in a scintillator and of the visible light to electric charge in a photodetector, which most commonly is a photomultiplier tube (PMT) [1]. In positron emission tomography (PET), which is of particular interest to this study, the radiation quanta are antiparallel 511 keV photons that originate from annihilation of positrons emitted from specific β^+ radionuclides, typically ^{18}F. Even though there are efforts to replace this two-step process, and the associated information loss, with a semiconductor detector material which has direct conversion of the 511 keV photon energy into charge in a single process [2], the scintillator-photodetector combination still remains the standard radiation detector used in PET.

Within the past decade there has been increased interest in semiconductor-based single photon counting devices, as an alternative photodetector architecture that can detect individual photons at visible wavelengths at a much higher quantum efficiency compared to PMTs [3,4]. These photodetectors currently find broad applicability in various research areas, such as telecommunications, physics and biomedical research [5–8]. Probing individual photons is desirable in many applications involving the detection of low levels of light, as well as in applications where the information that specific photons carry is critical. In the case of PET examples of

#139633 - $15.00 USD Received 14 Dec 2010; accepted 7 Jan 2011; published 13 Jan 2011

such information are the arrival time of the scintillation photon that has been detected first, or the correlation between that photon's arrival time and its point of origin within the scintillation crystal (otherwise known as depth of interaction or DoI). The architecture of arrays of single photon counting devices is such that optimum performance is observed for given characteristics of the optical stimulus, such as moderate intensity and short duration. Stimuli originating from coherent light sources allow for tunability of their intensity and duration to values that will guarantee optimum photodetector response.

In this study we focus our research in biomedical applications that use Si-based single photon detector arrays to detect spatially and temporally incoherent optical photons emitted during a scintillation process. However, the results can be applicable for a response to a different luminescence process as well. The properties of such optical stimuli deviate significantly from aforementioned desired ones, thus leading to non-optimum photodetector response. The response of single photon counting arrays to incoherent light has not been extensively studied, yet a general understanding of the different factors that contribute to signal formation is highly desired. This holds true especially in the case of PET, that seeks to detect pairs of simultaneously emitted annihilation quanta based on the generated signals upon their absorption to two scintillation detector elements located on opposite sides of the patient. In this case the response of photodetectors to scintillation light is affected by a number of systematic and random effects which should be properly identified in order to accurately reflect the quanta arrival time. In a recent study we have performed simulations and experiments that outline the dependence of the accuracy at which the arrival time information is estimated on scintillator-specific attributes, such as crystal length, surface treatment, light yield, as well as DoI [9].

In this work we present and evaluate a model of the response to scintillation of single photon counting arrays with focus on silicon photomultipliers (SiPMs). The ultimate goal of this study is to extend existing knowledge to a more in-depth understanding of the factors that contribute to signal formation in arrays of single photon detectors and to determine under which circumstances deviation from optimal performance is observed. The basic features of the SiPM model were adopted by [10] and properly modified to simulate a complete SiPM instead of individual microcells. Although there have been several studies modeling the stimulated response of isolated microcells in conjunction with an equivalent circuit that represents non-stimulated microcells of the SiPM [11–13], these studies typically assume simultaneous optical stimuli for each microcell (such as the ones emitted from a laser source or a light emitting diode). Contrarily, in the current study a dedicated model of each microcell within a SiPM is developed and its response to a realistic scintillation stimulus, as simulated by an appropriate optical model, is monitored on a photon-by-photon basis. The findings will be useful in the imaging field in order to guide the design of future scintillation detectors for PET as well as other biomedical applications.

2. Silicon photomultipliers with passive quenching

Semiconductor single photon counting arrays, known with various acronyms such as silicon photomultipliers (SiPMs), multi-pixel photon counters (MPPCs), solid state photomultipliers (SSPMs) and single photon avalanche diodes (SPADs), are arrays of avalanche photodiodes (APDs) operating above breakdown in Geiger mode. The individual Geiger APDs (GAPDs), otherwise known as microcells, are connected in parallel to form an array of several thousands of microcells per mm^2 of photosensitive area (Fig. 1, left).

When assuming a low photon flux incident to the SiPM, the device is able to generate a total signal which is proportional to the optical photon intensity. Signal formation in SiPMs is based upon the effective pile-up of the single photoelectron pulses. For the case of instant optical stimulus the SiPM response is maximized, however in the case of time variant optical inten-

#139633 - $15.00 USD Received 14 Dec 2010; accepted 7 Jan 2011; published 13 Jan 2011

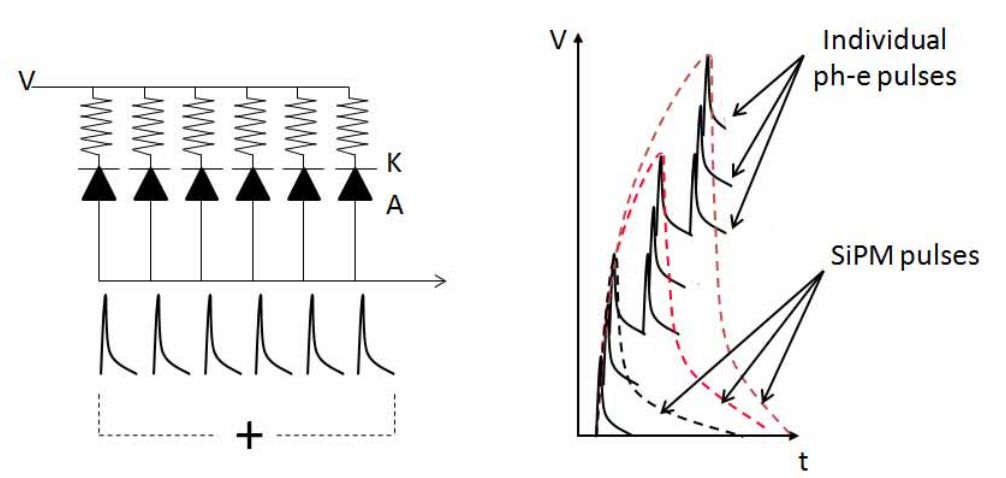

Fig. 1. Left: Schematic of the basic architecture of a SiPM consisting of multiple passively-quenched Geiger APDs (microcells) connected in parallel. Right: The individual photoelectron pulses from each microcell (solid lines) arrive asynchronously and are summed in a common readout line to form the SiPM pulse (dashed lines) as a result of their effective pile-up. Figure adopted from [14].

sity, such as a scintillation stimulus, the SiPM response is subject to variations and statistical uncertainties due to the inefficient single photoelectron pulse pile-up (Fig. 1, right).

Depending on the quenching mechanism used, the single photoelectron pulse properties and the pile-up of many subsequent such pulses may vary [15–18]. The focus of this work is in SiPMs employing passive quenching given their currently larger availability. For a passively quenched SiPM the decay time of the single electron pulses may consist of two components, as seen in Eqs. (1) and (2):

$$\tau_{ph,decay,1} \sim R_{load} \cdot (C_{trace} + N \cdot \frac{C_{quench} \cdot C_{diode}}{C_{quench} + C_{diode}}) \quad (1)$$

$$\tau_{ph,decay,2} \sim R_{quench} \cdot (C_{quench} + C_{diode}) \quad (2)$$

where R_{quench} and C_{quench} are the passive elements of the quenching circuitry, C_{diode} is the individual microcell capacitance, C_{trace} is the readout trace parasitic capacitance and R_{load} is the load impedance at which the SiPM is connected for readout.

One of the two components is associated with the diode recovery time ($\tau_{ph,decay,2}$), whereas the other component ($\tau_{ph,decay,1}$) is associated with the total impedance "seen" by each microcell, namely the impedance of the microcells as well as the input load of the subsequent readout electronics. For typical values of the passive elements $\tau_{ph,decay,2}$ is a slow decay component compared to $\tau_{ph,decay,1}$, however depending on the values of C_{diode} and C_{quench} the role of the two decay times as fast/slow components may be inverted.

The rise time of the single electron pulses is more difficult to describe mathematically. It primarily depends on the avalanche duration, which for silicon is estimated to be a few hundreds of ps, and is limited by the input bandwidth of the readout electronics.

#139633 - $15.00 USD Received 14 Dec 2010; accepted 7 Jan 2011; published 13 Jan 2011

3. Model of SiPM response to a scintillation optical signal

3.1. Convolution model - theory

In theory, the signal formed by a SiPM when stimulated by scintillation photons can be described by the convolution of the single SiPM microcell response probability density function ($\text{pdf}_{PD\ microcell}$) and the scintillation pdf ($\text{pdf}_{scintillation}$), as described in Eqs. (3), (4) and (5).

$$pdf_{detector} = pdf_{scintillation} \otimes pdf_{PD\ microcell} \tag{3}$$

$$pdf_{scintillation} = random\left(\frac{1}{\tau_{sc,decay} - \tau_{sc,rise}} \cdot \left(e^{-\frac{t}{\tau_{sc,decay}}} - e^{-\frac{t}{\tau_{sc,rise}}}\right), PDE\right) \tag{4}$$

$$pdf_{PD\ microcell} = \frac{1}{\tau_{ph,decay,1} + \tau_{ph,decay,2} - \tau_{ph,rise}} \cdot \left(e^{-\frac{t}{\tau_{ph,decay,1}}} + e^{-\frac{t}{\tau_{ph,decay,2}}} - e^{-\frac{t}{\tau_{ph,rise}}}\right) \tag{5}$$

where $\tau_{sc,decay}, \tau_{sc,rise}$ ($\tau_{ph,decay,1}, \tau_{ph,decay,2}, \tau_{ph,rise}$) are the decay and rise time constants, respectively, of the scintillator (photodetector). The function random(..,PDE) is a random number generator following the binomial distribution with probability of success equal to the value of the parameter PDE which represents the SiPM photon detection efficiency. The role of this function is to emulate the limitations imposed in the photodetector response to the detected scintillator pdf due to the relatively low photon detection efficiency of the former typically ranging from 10% to 50% [19]. Examples of the analytically derived pdfs based on Eqs. (4) and (5) are shown in Fig. 2.

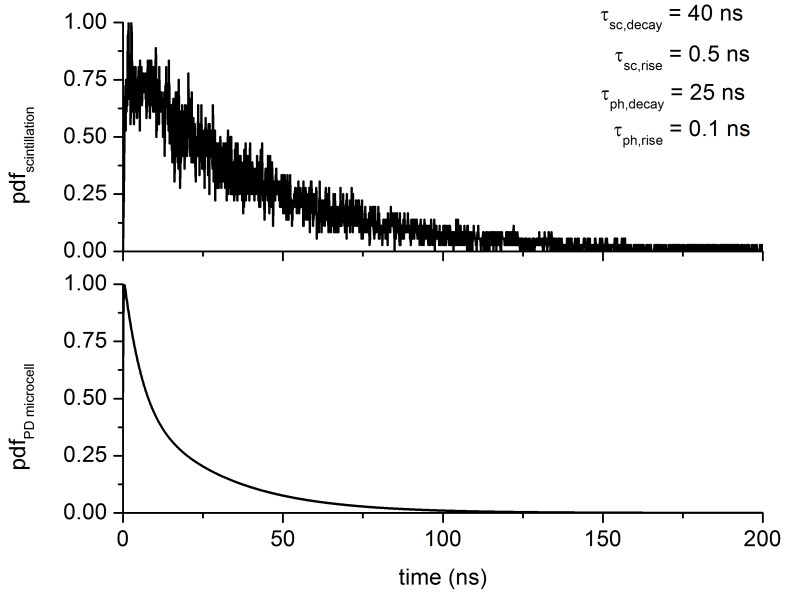

Fig. 2. Examples of $\text{pdf}_{scintillation}$ and $\text{pdf}_{PD\ microcell}$ calculated from Eqs. (4) and (5) for a 40 ns/0.5 ns scintillation decay/rise time and for a 25 ns/0.1 ns photodetector microcell rise/decay time. The pdfs are normalized to their maximum values for illustration purposes.

Based on the theory of passive quenched SiPMs presented in Section 2 the pdf describing the photodetector response (Eq. (5)) has two different decay constants related to the discharge and the recovery of the diode. Table 1 shows different values for the $\tau_{ph,decay,1}, \tau_{ph,decay,2}$ for varying

#139633 - $15.00 USD Received 14 Dec 2010; accepted 7 Jan 2011; published 13 Jan 2011

combinations of the values for C_{diode} and C_{quench}. It is noted that for all combinations the $\frac{C_{quench}}{C_{diode}}$ value ratio is kept constant in order to simplify the parametrization of the photodetector microcell response pdf.

Table 1. Values for the two decay components of the photodetector response considered in theory and the optical-electrical model. The first two columns show the values for capacitances C_{diode} and C_{quench} chosen as input to Eqs. (1) and (2)

C_{diode} (fF)	C_{quench} (fF)	$\tau_{ph,decay,1}$ (ns)	$\tau_{ph,decay,2}$ (ns)
120	40	8.15	48
60	20	5.45	25
24	8	3.83	9.6
12	4	3.29	4.8
2.4	0.8	2.86	0.96

Since, according to Eqs. (1) and (2), for given values of R_{load}, R_{quench} and C_{trace} there is a single set of derived values for $\tau_{ph,decay,1}$ and $\tau_{ph,decay,2}$, in the following the photodetector microcell decay time will be denoted with the single term $\tau_{ph,decay}$, equal to $\tau_{ph,decay,2}$, while $\tau_{ph,decay,1}$ can be easily derived from the data of Table 1.

3.2. Optical electrical model - simulation

The process of signal formation in SiPMs has been electrically simulated using the LTspice simulation package [20]. Figure 3 shows a schematic model of a single microcell subcircuitry (Fig. 3 inset) as well as of an array of an arbitrary number of microcells (N).

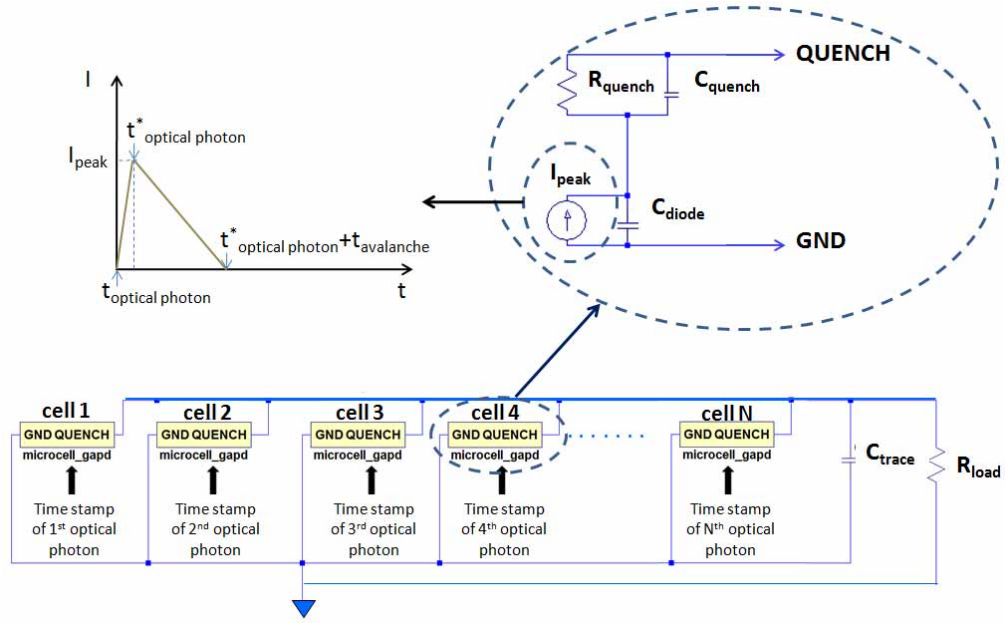

Fig. 3. Schematic representation of the combined optical-electrical model used to predict the SiPM response to scintillation light. Each microcell is modeled as a current source triggered at a time point equal to the time stamp of each sequentially detected scintillation photon ($t_{optical\ photon}$). The amplitude of the charge delta function (I_{peak}) has been selected to emulate a SiPM of a specific gain at a typical overvoltage of 2 V. For this study the number of simulated microcells (N) is 3600.

#139633 - $15.00 USD Received 14 Dec 2010; accepted 7 Jan 2011; published 13 Jan 2011

Each microcell is essentially modeled in LTspice as a current source producing a charge spike which ideally emulates a delta function. However, in order to include in the model the finite duration of the avalanche mechanism (including breakdown and quenching), the current source output is mathematically described by a piece-wise linear function defined at three (t,I) coordinate pairs (Fig. 3):

$$\begin{aligned}(t_{start}, I_{start}) &= (t_{optical\ photon}, 0)\\ (t_{peak}, I_{peak}) &= (t^{*}_{optical\ photon}, I_{peak})\\ (t_{stop}, I_{stop}) &= (t^{*}_{optical\ photon} + t_{avalanche}, 0)\end{aligned}$$

where $t_{optical\ photon}$ is the flight time information of each detected optical photon used to initiate a current pulse in each microcell, $t^{*}_{optical\ photon}$ is equal to $t_{optical\ photon}$ temporally shifted to an "infinitesimally" small distance (equal to 1 ps in the current model) in order to emulate instant current generation and $t_{avalanche}$ is the duration of the avalanche mechanism. Information about the value of $t_{optical\ photon}$ is provided by performing an optical tracking simulation of a given number of scintillation photons emitted according to a pdf similar to $pdf_{scintillator}$ (Eq. (4)) with the difference that the SiPM PDE contribution is not included. The path of each simulated photon within the confined volume of a rectangular crystal element is tracked and the time elapsed from generation to detection is registered. The optical simulation package used is DETECT2000 [21].

As seen in the top left illustration of Fig. 3, although the shape of the current source response lacks symmetry around a central time point, as would be required if the response was an ideal delta function, its temporal width always approximates the value of $t_{avalanche}$. The asymmetry was introduced in order to include the abrupt transitions below breakdown due to the avalanche quenching mechanism.

The value of I_{peak} is determined based on calculations of the total amount of charge produced during the avalanche process as given by the following equation:

$$Q = (C_{cell} + C_{quench}) \cdot (V_{bias} - V_{breakdown}) \tag{6}$$

and published results on the duration of the avalanche process in silicon [22, 23]. $V_{breakdown}$ is the breakdown voltage which for the specific diodes under study is around 69 V, while V_{bias} is the applied voltage at the SiPM terminals (on the order of 71 V for the device under study). Knowing the values of Q and $t_{avalanche}$ an approximate estimation of I_{peak} is given by:

$$I_{peak} = \frac{Q}{t_{avalanche}} \tag{7}$$

The current source is connected in parallel with a small capacitance (C_{diode}) which represents the SiPM inherent diode capacitance. The pulse then goes through a resistor-capacitor network (R_{quench}-C_{quench}) which represents the avalanche quenching circuitry.

Each microcell subcircuitry, as described above, is connected in parallel with all the others using readout traces which contribute to a parasitic capacitance (C_{trace}) and the sum of the individual charge spikes (single photoelectron pulses) is read out with a resistive load of variable value (R_{load}). The values for C_{diode},R_{quench},C_{quench} and R_{load} are summarized in Table 2.

Alternative studies model the SiPM microcells as voltage sources connected in parallel with a resistor, where the avalanche process is triggered by a controlled switch [12]. For the purpose of determining the overall SiPM response to scintillation light, the approach of a microcell as a current or voltage source is considered equivalent, despite the different information content that can be derived in either approach.

In order to include the finite photon detection efficiency (PDE) of the SiPM, each optical photon that meets the detection criteria (i.e manages to reach the photodetector sensitive area)

#139633 - $15.00 USD Received 14 Dec 2010; accepted 7 Jan 2011; published 13 Jan 2011

Table 2. The various simulation parameters used in the optical electrical model

parameter	value
n (optical photons)	14000
$\tau_{sc,rise}$ (ns)	0.1-5
$\tau_{sc,decay}$ (ns)	1-50
N (microcells)	3600
I_{peak} (mA)	1.5
$t_{avalanche}$ (ps)	100
C_{diode} (fF)	2.4-120
R_{quench} (kOhm)	300
C_{quench} (fF)	0.8-40
C_{trace} (pF)	55
R_{load} (Ohm)	50

during the optical simulation is passed through an additional decision procedure based upon a Bernoulli statistical process which essentially is a binomial distribution with a single trial and 40% probability of success. The complete simulation process is summarized in the block diagram of Fig. 4. Recovery time effects and geometrical considerations in this study are taken into account within the 40% PDE assumed for the SiPM.

4. Simulation results

The optical electrical simulation results are initially compared with theoretical predictions based on a the convolution model (theory) described in Section 3.1 and subsequently validated with the experimentally measured scintillator-photodetector response. In both theory and simulation the dependence of decay/rise time and maximum amplitude of the detector response is studied as a function of the photodetector decay time and the scintillator rise and decay times. In every case that the detector response is studied as a function of one variable, all the other variables are assigned fixed values which are summarized in Table 3. These values were se-

Table 3. The fixed values assumed for the variables $\tau_{sc,rise}$, $\tau_{sc,decay}$, $\tau_{ph,rise}$,$\tau_{ph,decay}$

variable	value
$\tau_{sc,rise}$ (ns)	0.5
$\tau_{sc,decay}$ (ns)	40
$\tau_{ph,rise}$ (ns)	0.1
$\tau_{ph,decay}$ (ns)	25

lected under the assumption that they represent a good approximation to the values quoted in literature for lutetium oxyorthosilicate (LSO) crystals [24], which are widely used in PET, and SiPM photodetectors [25].

4.1. Convolution model - theory

Figure 5 shows the theoretically predicted scintillator-photodetector response for different scintillator rise/decay times ($\tau_{sc,rise}$, $\tau_{sc,decay}$ in Eq. (4)) and photodetector decay times ($\tau_{ph,decay}$ equal to $\tau_{ph,decay,2}$, in Eq. (5)). The signal amplitudes (y-axis) have been normalized to the maximum value at each graph in order to observe the relative changes in pulse height for different values of the rise and decay times.

The predictions of both theory, as well as the developed optical electrical model, for varying microcell rise times are not included in this study given the difficulties of accurately describing the processes affecting this variable. However, it is expected that the effects of detector response associated with the microcell rise time will be similar to the effects associated with

#139633 - $15.00 USD Received 14 Dec 2010; accepted 7 Jan 2011; published 13 Jan 2011

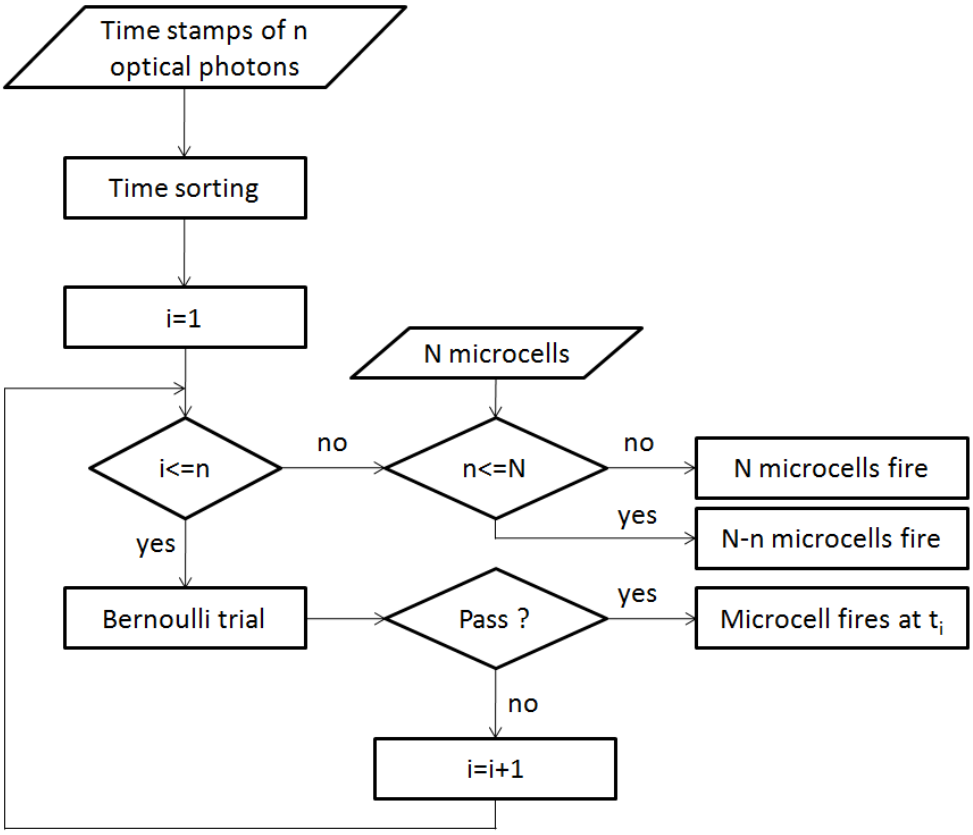

Fig. 4. Flow chart of the combined optical electrical detector model. An analytically implemented Bernoulli decision process is used to emulate the limited SiPM PDE and an iterative comparison between the number of scintillation photons n and the number of microcells N is performed at each step to ensure that the dynamic range limits of the SiPM have not been surpassed.

the scintillator rise time (Fig. 5, top left).

4.2. Optical electrical model - simulation

Figure 6 shows the scintillator-photodetector response predicted by the optical electrical model for different scintillator rise/decay times and photodetector decay times. The scintillator rise and decay times are varied within the DETECT2000 simulation which models the scintillator response with a pdf similar to the one described in Eq. (4). Within the LTspice simulation the photodetector microcell decay time is adjusted by changing the values of C_{diode} and C_{quench} while keeping R_{quench} and R_{load} fixed in order to avoid insufficient quenching of the microcell current as well as variations on the observed pulse height due to variations in the resistive load.

In the case of variable photodetector decay time (Fig. 6, bottom), the effect of the microcell pulse pile-up becomes evident; even though for decreasing $\tau_{ph,decay}$ the detector response is characterized by higher amplitude and smaller rise/decay times, it also appears to have larger pulse height fluctuations. This effect is attributed to the ineffective pile-up of microcell pulses induced by subsequent optical photons which is more enhanced if the arrival time of an optical photon does not overlap with the recovery time of a previously induced microcell. The bottom

#139633 - $15.00 USD Received 14 Dec 2010; accepted 7 Jan 2011; published 13 Jan 2011

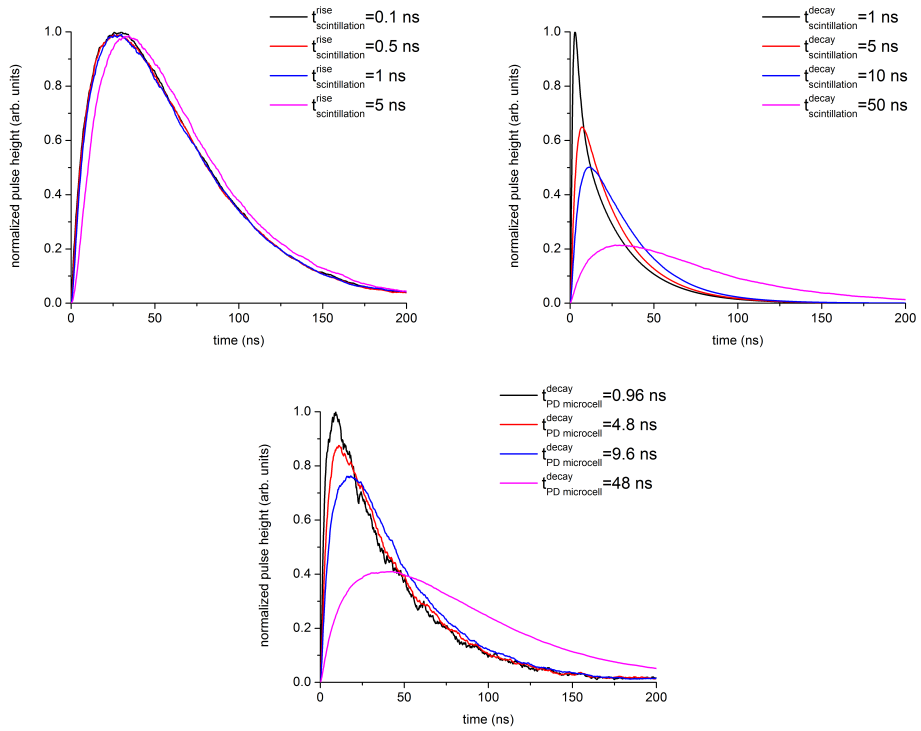

Fig. 5. Scintillation induced response of a SiPM based on the convolution of a pdf describing the scintillator response and a pdf describing the photodetector microcell response. The modeled response is shown as a function of scintillator rise (top left), scintillator decay (top right) and SiPM microcell decay (bottom). In each graph all the rise/decay times of the scintillator/photodetector microcell that are not varied, are given constant values shown in Table 3.

plot of Fig. 6 also shows that for a sufficiently large microcell decay time the pulse height fluctuations are smaller (due to more effective pile-up), despite the significantly smaller pulse height. The validity of this effect is also verified in theory (bottom plot of Fig. 5).

In the case of variable scintillator decay time (Fig. 6, top right) an adverse effect is observed where an increasing $\tau_{sc,decay}$ leads to decreasing pulse height and increasing pulse height fluctuations. Similar to the convolution model (Fig. 5, top left), the scintillator rise time does not appear to have a significant effect in the overall detector response as seen from the top left plot of Fig. 6.

5. Model validation

5.1. Comparison with theory

Figure 7 shows comparative graphs of the dependence of maximum pulse height, as calculated from the modeled responses of Figs. 5 and 6, as a function of scintillator and photodetector decay times for the theoretical and the optical electrical model, respectively. Also shown in this figure, are the dependence of the calculated rise and decay times of the overall detector response as a function of the same parameters. Similar trends are observed in both theory and simulation with observable deviations that can be attributed to the fact that the theoretical formulas in

#139633 - $15.00 USD Received 14 Dec 2010; accepted 7 Jan 2011; published 13 Jan 2011

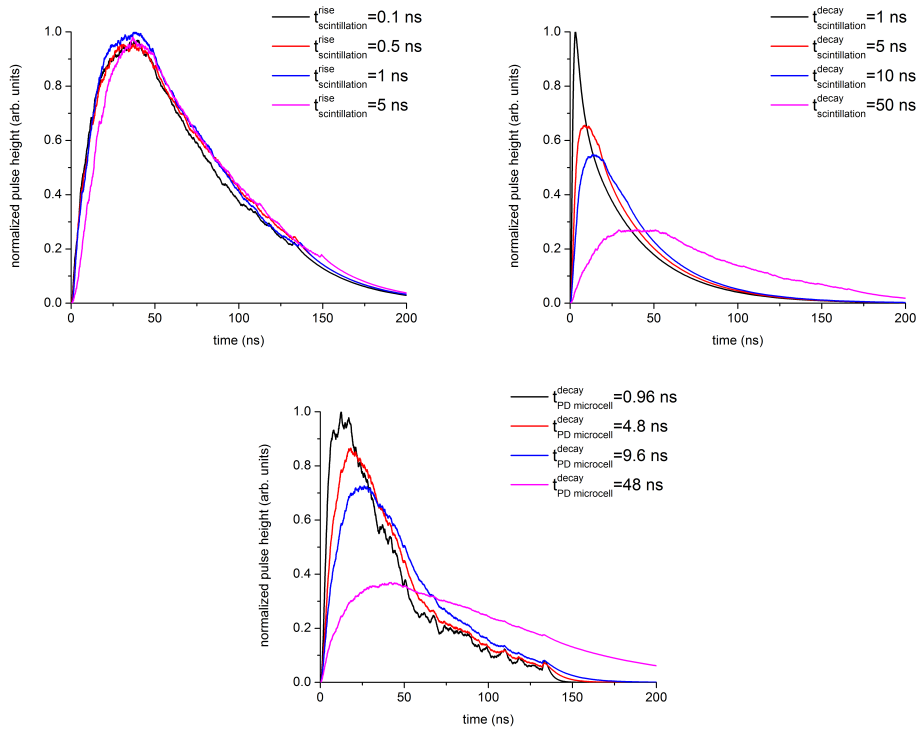

Fig. 6. Scintillation induced response of a SiPM based on the simulation process shown in Figure 3. The modeled response is shown as a function of scintillator rise (top left), scintillator decay (top right) and SiPM microcell decay (bottom). In each graph all the rise/decay times of the scintillator/photodetector microcell that are not varied, are given constant values shown in Table 3.

Eqs. (3), (4) and (5) can provide a generalized framework to predict the detector response, however they do not take into account the various physical and electrical effects encountered in the optical electrical model.

5.2. Comparison with measurement

Validation of the optical electrical model with experimental results has been performed by acquiring signals generated from a LSO-SiPM radiation detector, upon absorption of annihilation quanta emitted from a ^{22}Na positron source. The scintillation material used was Ca co-doped (0.4% Ca concentration) LSO with a measured decay time of 30 ns [24]. The photodetector is a Si-based, blue enhanced 3×3mm^2 MPPC consisting of 3600 microcells (Hamamatsu). The experimental setup used for these measurements is shown in Fig. 8.

In order to compare with the modeled LSO-SiPM response, the detector attributes in both measurements and the model have been appropriately adjusted. The response is measured and simulated when the LSO crystal ($3 \times 3 \times 20$ mm^3, polished surfaces) is irradiated from the side at a point located in the middle of the scintillation crystal element. While in the optical electrical model the exact point of optical photon generation within the crystal volume can be determined, in the case of measurement a second LSO-SiPM detector ($3 \times 3 \times 5$ mm^3, rough surfaces) is used to confine the interaction point by means of electronic collimation.

Figure 9 shows the predicted by the optical electrical model LSO-SiPM response (bottom

#139633 - $15.00 USD Received 14 Dec 2010; accepted 7 Jan 2011; published 13 Jan 2011

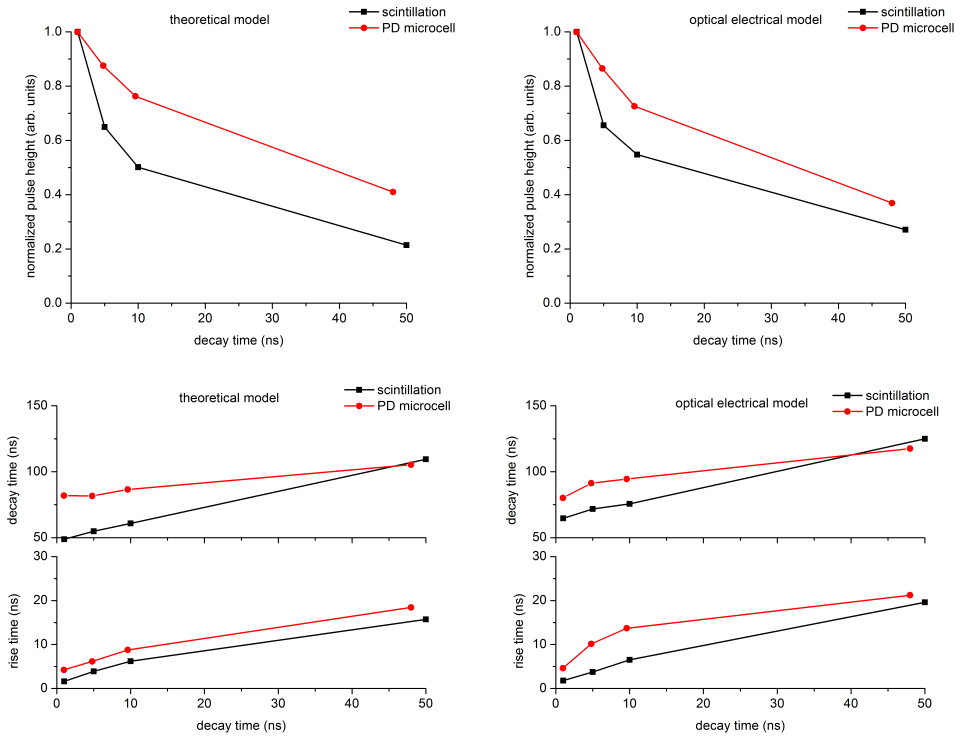

Fig. 7. Relative pulse height (normalized to the maximum value, top row of graphs) and decay/rise time (bottom rows of graphs) as a function of the scintillator (squares) and the photodetector microcell (circles) decay time. Results are shown for both the theoretical model (left) and the optical electrical simulation model (right).

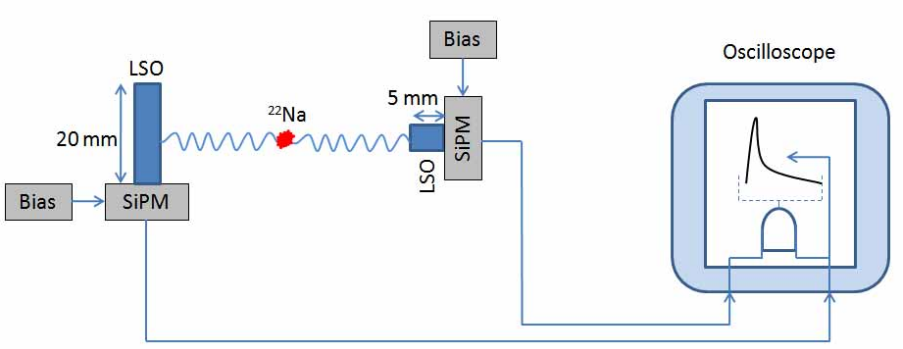

Fig. 8. Schematic of the experimental setup for the measurement of a scintillator-photodetector response to the absorption of annihilation quanta. Signals from a 20 mm length LSO crystal read out by a SiPM are digitized with a fast oscilloscope. The bitwise AND operation symbol appears in the oscilloscope screen in order to demonstrate that the signals from the 20 mm length detector are digitized only under the concurrent presence of a signal from the opposing 3 mm length detector.

graph) over 25 generated responses for a different seed of the random number generator at each

#139633 - $15.00 USD
Received 14 Dec 2010; accepted 7 Jan 2011; published 13 Jan 2011

case. The same figure also shows the measured persistence view of 50 detector signals (top graph). Due to the design of the experimental setup the signal appears to be bipolar owing to the RF filtering of the SiPM bias voltage. In order for the signals to be fully comparable we have added in the optical electrical simulation a similar filter circuit.

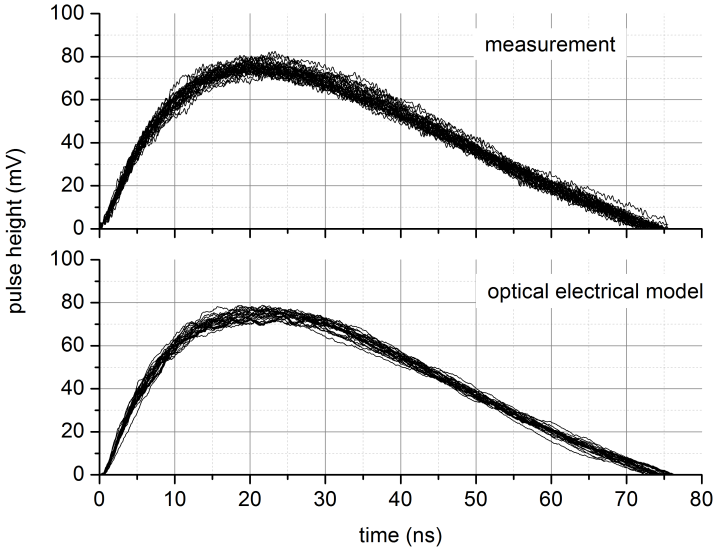

Fig. 9. Comparison between the measured persistence oscilloscope waveform caption over 50 LSO-SiPM detector pulses (top) and 25 simulated detector pulses (bottom). In measurement, a 20 mm length scintillation crystal has been irradiated from the side with a ^{22}Na source and an interaction depth in the middle of the crystal was achieved through electronic collimation. In simulation, scintillation photons were generated in the middle of a 20 mm length crystal and the arrival times of the detected photons were used to generate a response in the SiPM according to the logic described in Fig. 4.

It should be noted that although the optical electrical model does not include the energy resolution of the LSO-SiPM detector (which generally is a function of the scintillation crystal intrinsic energy resolution, the photodetector multiplication noise and the noise of the acquisition electronics), a visual comparison in the persistence views of the simulated and the measured responses yields comparable results.

A more quantitative comparison of the two responses can be made by comparing the average detector response in each case, as shown in the top graph of Fig. 10. The error bars are based on the calculated standard deviation values of the mean response and in the case of measurement they are indicative of the detector energy resolution, while in the case of simulation are indicative of statistical variations in photon detection. The experimentally derived and simulated values have a systematic temporal shift due to the different sampling pattern adopted by the digitizing electronics (in the case of measurement) and by the simulation transient analysis (in the case of the optical electrical model). Trace interpolation at the same time points was performed in order to allow for direct comparison between the two cases.

The bottom graph of Fig. 10 shows the calculated difference of the two average responses at each time bin. The error bars are calculated based on the error propagation formula for the subtraction of two independent quantities, and are dominated by the error indicative of the

#139633 - $15.00 USD Received 14 Dec 2010; accepted 7 Jan 2011; published 13 Jan 2011

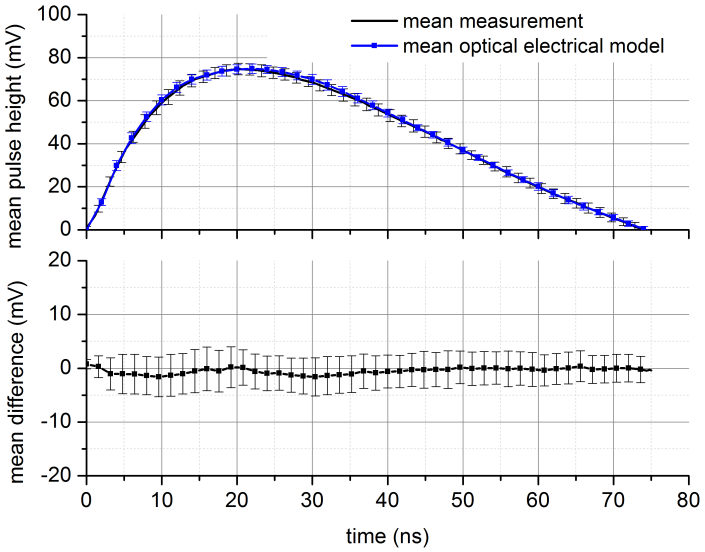

Fig. 10. Top: the mean scintillation-induced SiPM response averaged over 50 measured signals (black) and over 25 modeled signals (blue). Bottom: the difference between the measured and simulated signals of top plot.

detector energy resolution included in the measured LSO-SiPM response. The graph shows a difference close to zero with deviations observed when the response is around its peak value. These deviations are however within the estimated simulation error.

The calculated values of maximum pulse height, rise and decay times of the simulated and the measured detector response are summarized in Table 4. The errors quoted in the case of

Table 4. Comparison between measured values and values estimated by the optical electrical model

variable	measurement	optical electrical model
maximum pulse height (mV)	76.6±2.5	76.1±1.8
10%-90% rise time (ns)	11.1±1.1	11.1±0.9
90%-10% decay time(ns)	35.8±2.2	36.5±1.8

the simulated and measured response are calculated as standard deviation over all 25 simulated and 50 acquired traces, respectively. As seen from the table the simulation predictions are in excellent agreement with the measurement, thus verifying the validity of the developed optical electrical model. The calculated mean deviation of the optical electrical model over measurement is 1% for all three variables considered in Table 4 (maximum pulse height, rise and decay time). The agreement in the calculated and simulated value of the maximum pulse height is remarkable given the fact the the optical electrical model does not include the scintillator intrinsic resolution of approximately 7% for Ca co-doped (0.4% concentration) LSO [26]. This strongly suggests that the scintillation induced signal formation process in Si-based single photon counting arrays is subject to statistical fluctuations that are comparable to the inherent statistical nature of scintillation light emission.

#139633 - $15.00 USD Received 14 Dec 2010; accepted 7 Jan 2011; published 13 Jan 2011

6. Conclusion

This study presents the feasibility of a complete optical electrical model used to simulate the signal formation of a scintillation detector consisting of Si-based arrays of single photon counters. Validation with both theoretical calculations as well as measurements show that the model can accurately predict the response of SiPM single photon counting arrays to scintillation light. This model can be used as a tool to further understand the dependence of this response on basic detector characteristics, such as rise and decay time of the scintillator/photodetector, and can help to understand the contributions of each component to important performance parameters, such as light output and time resolution.

In addition, the combination of optical and electrical properties of the detector under the same simulation framework may allow for more accurate correlation of unknown parameters at the scintillation level to well defined parameters at the electrical response level by using appropriate signal processing techniques. Such correlation is highly desired in imaging modalities such as time of flight PET (ToF-PET), where accurate extraction of timing information has shown to depend on a variety of detector parameters in both the crystal and photodetector level [9].

It is expected that the findings of this study will guide the selection of the best combination of attributes that will optimize performance in scintillation detection. We aim at using the developed optical electrical model to guide the design of future radiation detectors in PET. Especially given the dominating trend in PET technology towards continuous, full detector signal digitization, models such as the one presented in this work will enhance the effort to extract the maximum amount of information based on signal processing methods and corrections.

Future work involves optimization of the model in order to properly account for detector response changes under the presence of optical crosstalk [27], afterpulses and dark counts [28]. The prediction of the detector response shape at the non-linear regime is currently under study given the improved timing performance of the devices under operating conditions near device saturation.

Acknowledgments

The authors would like to thank Dr. Chuck Melcher (University of Tennesse, USA) for providing the Ca co-doped LSO scintillation crystal. This work is supported in part by the AXA Research Fund.

#139633 - $15.00 USD Received 14 Dec 2010; accepted 7 Jan 2011; published 13 Jan 2011